Port-Hamiltonian Flight Control of a Fixed-Wing Aircraft

Jean-Michel Fahmi, *Student Member, IEEE*, and Craig A. Woolsey, *Senior Member, IEEE*

***Abstract*— This brief addresses the problem of stabilizing steady, wing level flight of a fixed-wing aircraft to a specified inertial velocity (speed, course, and climb angle). The aircraft is modeled as a port-Hamiltonian system and the passivity of this system is leveraged in devising the nonlinear control law. The aerodynamic force model in the port-Hamiltonian formulation is quite general; the static, state feedback control scheme requires only basic assumptions concerning lift, side force, and drag. Following an energy-shaping approach, the static state feedback control law is designed to leverage the open-loop system's port-Hamiltonian structure in order to construct a control Lyapunov function. Asymptotic stability of the desired flight condition is guaranteed within a large region of attraction. Simulations comparing the proposed flight controller with dynamic inversion suggest it is more robust to uncertainty in aerodynamics.**

***Index Terms*— Flight vehicle dynamics, Lyapunov methods, nonlinear control systems, port-Hamiltonian systems (PHSs).**

I. Introduction

CONVENTIONAL approaches to flight control of fixed-wing aircraft rely on linearizing the vehicle dynamics about an equilibrium motion, such as wings-level flight at constant altitude and speed. The utility of control schemes, such as linear quadratic or $\mathcal{H}_\infty$ control, that rely on a small perturbation model is limited to a neighborhood of the nominal flight condition. One can develop a family of controllers that are parameterized by the desired speed, climb angle, etc., but the performance and stability of the resulting closed-loop system will generally depend on the rate of parameter variation.

To obtain effective closed-loop performance with stability guarantees over a larger operating envelope, one may instead consider nonlinear control design methods such as dynamic inversion [1]–[3] or adaptive control [4]–[6]. Dynamic inversion, or feedback linearization, requires a well-characterized model of nonlinear dynamics. Such a model may be impractical to obtain over the full flight envelope, particularly for an aircraft whose configuration and inertial parameters vary substantially between flights. Model reference adaptive control and adaptive backstepping can accommodate a variety of uncertainties, including uncertain nonlinearities, assuming the system satisfies certain structural conditions. The resulting dynamic state feedback controllers are often computationally sophisticated, however, which can limit their utility for low-cost platforms such as small unmanned aircraft.

The design proposed in this brief is based on modeling the aircraft as a port-Hamiltonian system (PHS) [7], an extension of Hamiltonian systems in classical mechanics to systems with inputs, outputs, and dissipative forces. PHSs are characterized by a scalar function representing the total energy of the system along with a pair of matrix functions that describe how energy is distributed and dissipated. Modeling the system as a PHS facilitates nonlinear, energy-based control design and allows using established energy-shaping techniques for PHS [8], such as interconnection and damping assignment, passivity-based control (IDA-PBC) [9]. Passivity-based control (PBC) has proven to be effective in various applications such as the control of electric motors [10] and quadrotors [11]–[15].

Of the many mechanical system applications of PBC described in the current literature, perhaps the closest to the proposed application of fixed-wing aircraft flight control is the use of PBC to control unmanned underwater vehicles (UUVs). Woolsey [16] developed a cross-track control law for a slender, underactuated UUV using potential energy shaping. Fahmi and Woolsey [17] adapted this notion of potential energy shaping for directional stabilization of a fixed-wing aircraft. The closed-loop performance, however, exhibited undesirable excursions in the aerodynamic angles, particularly in the sideslip. In a different approach to energy shaping, Valentinis *et al.* [18] developed a feedback controller for a slender, underactuated UUV by shaping the target dynamics, and suppressing the influence of unactuated degrees of freedom. In [19], Valentinis *et al.* expanded the scope of control design to include precision guidance along a helical trajectory. More recently, Valentinis and Woolsey [20] developed a PBC for a non-neutrally buoyant, underactuated submarine executing an emergency ascent.

With the exception of [20], the studies mentioned above ignore the force of gravity, which is balanced by buoyancy. While hydrodynamic forces such as lift and drag certainly affect underwater vehicle motion, the nominal state of motion is to advance at a constant speed with minimum drag and zero lift, so hydrodynamic forces can be treated as perturbations to be rejected by the control system. In contrast, fixed-wing aircraft rely on an aerodynamic lift to counter the gravitational force in steady flight and to execute maneuvers. The work presented in this brief focuses on stabilizing the aircraft velocity by exploiting some remarkable properties of the aerodynamic force when expressed in a port-Hamiltonian framework. The approach to control design is

Manuscript received May 10, 2020; revised December 16, 2020; accepted February 8, 2021. Manuscript received in final form February 15, 2021. This work was supported in part by the National Science Foundation under Grant CNS-1650465 and in part by the National Aeronautics and Space Administration (NASA) under Grant 80NSSC20M0162. Recommended by Associate Editor A. Serrani. *(Corresponding author: Craig A. Woolsey.)*

The authors are with the Kevin T. Crofton Department of Aerospace and Ocean Engineering, Blacksburg, VA 24061 USA, and also with the Virginia Tech, Blacksburg, VA 24060 USA (e-mail: fahmi@vt.edu; cwoolsey@vt.edu).

Color versions of one or more figures in this article are available at https://doi.org/10.1109/TCST.2021.3059928.

Digital Object Identifier 10.1109/TCST.2021.3059928

inspired by the canonical transformation approach proposed by Fujimoto *et al.* [21].

The brief is organized as follows. Section II describes the structure of a PHS and summarizes the control design approach of Fujimoto *et al.* [21]. Section III presents the rigid body model for a fixed-wing aircraft, including a novel representation of the aerodynamic force in the PHS framework. The aerodynamic force model is quite general, so the resulting control strategy is effective for widely varying geometries. Section IV describes the application of the method presented in Section II to the model presented in Section III. Section IV gives concluding remarks.

II. Port-Hamiltonian Systems

The trajectory tracking control design method described by Fujimoto *et al.* [21], which serves as the basis for the control design presented in this brief, is based on a general theoretical framework for underactuated (electro-)mechanical systems. The approach relates to the IDA-PBC method described by Ortega *et al.* [9]; Fujimoto's [21] approach may be interpreted as a variant of the latter when the control system is time-invariant. Here, we briefly describe the structure of a PHS. A PHS has the form:

$$\dot{\boldsymbol{x}} = [\mathcal{J}(\boldsymbol{x}) - \mathcal{R}(\boldsymbol{x})]\frac{\partial \mathcal{H}}{\partial \boldsymbol{x}}^T + \boldsymbol{g}(\boldsymbol{x})\boldsymbol{u} \tag{1}$$

$$\boldsymbol{y} = \boldsymbol{g}^T(\boldsymbol{x})\frac{\partial \mathcal{H}}{\partial \boldsymbol{x}}^T \tag{2}$$

where $\boldsymbol{x}(t) \in \mathbb{R}^n$ is the state vector, $\mathcal{J}(\boldsymbol{x}) = -\mathcal{J}^T(\boldsymbol{x})$ is an interconnection matrix which represents energy conserving interactions among the state variables, the matrix $\mathcal{R}(\boldsymbol{x}) = \mathcal{R}^T(\boldsymbol{x}) \succeq 0$ accounts for the dissipation incurred during system motion, $\mathcal{H} : \mathbb{R}^n \to \mathbb{R}$ is the Hamiltonian function, and the matrix $\boldsymbol{g}(\boldsymbol{x}) \in \mathbb{R}^{n\times m}$ determines how the m inputs $\boldsymbol{u}(t) \in \mathbb{R}^m$ affect system motion. The input vector $\boldsymbol{u}(t)$ and the output vector $\boldsymbol{y}(t) \in \mathbb{R}^m$ are conjugate in the sense that their inner product expresses the power exchanged with external systems. The PHS can be shown to be passive [7] with the Hamiltonian as a storage function:

$$\frac{d\mathcal{H}(\boldsymbol{x})}{dt} = \boldsymbol{y}^T\boldsymbol{u} - \frac{\partial \mathcal{H}(\boldsymbol{x})}{\partial \boldsymbol{x}}\mathcal{R}(\boldsymbol{x})\frac{\partial \mathcal{H}(\boldsymbol{x})}{\partial \boldsymbol{x}}^T \leq \boldsymbol{y}^T\boldsymbol{u}. \tag{3}$$

Given a PHS model, the control design objective is to construct a passive error system through feedback transformation.

III. Vehicle Motion Model

We consider a rigid aircraft with four inputs: the thrust force and three control moments in roll, pitch, and yaw. Let $\boldsymbol{v} = [u, v, w]^T$ represent the translational velocity of the aircraft with respect to inertial space, but expressed in the body frame, and let $\boldsymbol{p} = [p_1, p_2, p_3]^T = m\boldsymbol{v}$ denote the corresponding body translational momentum, where m is the aircraft mass. Let $\boldsymbol{\omega} = [p, q, r]^T$ represent the angular velocity of the aircraft with respect to inertial space, but expressed in the body frame, and let $\boldsymbol{h} = [h_1, h_2, h_3]^T = \boldsymbol{I}\boldsymbol{\omega}$ denote the corresponding body angular momentum, where $\boldsymbol{I}$ is the moment of inertia matrix. It is convenient to define a transformation of the translational velocity variables $(u, v, w) \mapsto (V, \beta, \alpha)$ which is well-defined for $V > 0$ and $\beta \in (-\pi/2, \pi/2)$:

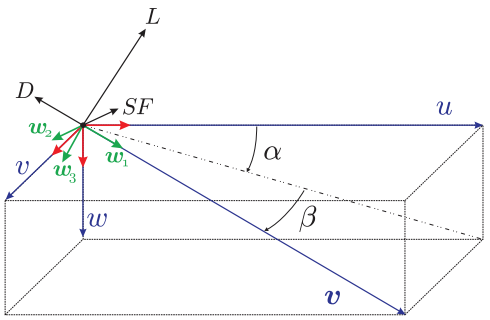

Fig. 1. Aerodynamic angles for an aircraft.

$$V = \|\boldsymbol{v}\|, \quad \beta = \arcsin\left(\frac{v}{V}\right), \quad \text{and} \quad \alpha = \arctan_4\left(\frac{w}{u}\right) \tag{4}$$

where $\arctan_4$ denotes the 4-quadrant arctangent (see Fig. 1). We can use the angle of attack, α, and sideslip angle, β, to define a proper rotation matrix mapping free vectors from a wind frame [22], where the aerodynamic forces are defined, to the body frame:

$$\mathbf{R}_{\mathrm{BW}}(\alpha, \beta) = e^{-\hat{\boldsymbol{e}}_2\alpha}e^{\hat{\boldsymbol{e}}_3\beta} \tag{5}$$

where $\boldsymbol{e}_i$ is the ith unit basis vector for $\mathbb{R}^3$ and the overhat indicates the 3×3 skew-symmetric "cross product equivalent matrix" which, for vectors $\boldsymbol{a}$ and $\boldsymbol{b}$, satisfies $\hat{\boldsymbol{a}}\boldsymbol{b} = \boldsymbol{a} \times \boldsymbol{b}$.

The aircraft orientation with respect to the inertial frame is typically expressed in terms of Euler angular rates corresponding to a common Euler angle parameterization for the rotation matrix $\mathbf{R}_{IB} = e^{\hat{\boldsymbol{e}}_3\psi}e^{\hat{\boldsymbol{e}}_2\theta}e^{\hat{\boldsymbol{e}}_1\phi}$. The rotational kinematic equations in this case are well-defined provided $\theta \neq \pm\pi/2$.

Alternatively, as described by Battista *et al.* [23], one may use the heading angle ψ together with the *tilt vector* $\boldsymbol{\zeta} = \mathbf{R}_{\mathrm{IB}}^T\boldsymbol{e}_3$ to describe the attitude kinematics. This alternative representation is well-defined provided $|\zeta_1| = |\boldsymbol{\zeta}^T\boldsymbol{e}_1| \neq 1$. That is, the parameterization is valid provided the body's forward axis is not aligned with the inertial vertical axis, precisely the same conditions under which the Euler angle parameterization holds. Thus, the aircraft rotational and translational kinematic equations are

$$\begin{aligned}\dot{\boldsymbol{\zeta}} &= \boldsymbol{\zeta} \times \boldsymbol{\omega}\\ \dot{\psi} &= -\left(1 - \zeta_1^2\right)^{-1}\boldsymbol{\zeta}^T\hat{\boldsymbol{e}}_1\hat{\boldsymbol{e}}_1\boldsymbol{\omega}\\ \dot{\boldsymbol{x}} &= \mathbf{R}_{\mathrm{IB}}\boldsymbol{v}.\end{aligned} \tag{6}$$

For flight in still air, the dynamic equations expressed in the body-fixed reference frame are

$$\dot{\boldsymbol{h}} = \boldsymbol{h} \times \boldsymbol{\omega} + \boldsymbol{\tau}_c + \boldsymbol{\tau}_a \tag{7}$$

$$\dot{\boldsymbol{p}} = \boldsymbol{p} \times \boldsymbol{\omega} + mg\boldsymbol{\zeta} + \boldsymbol{f}_c + \boldsymbol{f}_a \tag{8}$$

where $\boldsymbol{f}_a$ and $\boldsymbol{\tau}_a$ represent the aerodynamic force and moment, respectively, while $\boldsymbol{f}_c$ and $\boldsymbol{\tau}_c$ represent the control force and moment. We assume the aircraft has a single thruster aligned with its velocity such that $\boldsymbol{f}_c = F_c\,\boldsymbol{v}/V$, where F_c is the scalar thrust. The assumption that thrust is aligned with velocity is nonstandard—it would require a gimballed propulsor—but it resolves an analytical challenge in the coming stability

analysis. The assumption is revisited in Section V where we consider more conventional assumptions about thrust.

We assume the aerodynamic force and moment are governed by quasi-steady flow, depending only on the translational and rotational velocity. Rather than adopt explicit analytical expressions for aerodynamic effects, however, we make only generic assumptions. For example, we assume the aerodynamic moment opposes rotation and vanishes when the motion is purely translational: $\boldsymbol{\tau}_a \cdot \boldsymbol{\omega} < 0$ when $\boldsymbol{\omega} \neq \mathbf{0}$ and $\boldsymbol{\tau}_a = \mathbf{0}$ when $\boldsymbol{\omega} = \mathbf{0}$. In reality, there are important aerodynamic moments that arise from translational motion, such as the "weathervane" moments in pitch and yaw. Rather than account for these bare airframe effects early in the modeling process, we absorb them into the three-axis control moment to be defined shortly. To implement the resulting control law, one must first remove these moment contributions due to the aerodynamics of the bare airframe. A simple aerodynamic moment model that captures the primary effects of roll, pitch, and yaw damping is $\boldsymbol{\tau}_a = -\boldsymbol{D}_\omega(\boldsymbol{v})\boldsymbol{\omega}$ where $\boldsymbol{D}_\omega(\boldsymbol{v}) \succ 0$.

The aerodynamic force is typically expressed in wind frame components: the drag force, which opposes velocity; the lift force, which acts normal to drag and in the aircraft plane of symmetry; and the side force, which is normal to the two other components. These components are assumed to depend solely on the aerodynamic angles. In reality, small aerodynamic forces also arise in response to aircraft rotation. For example, an aircraft rotating in yaw will experience a small side force due to the vertical stabilizer; this small force, acting about the center of gravity through a large moment arm, provides a yaw damping moment. We ignore these small aerodynamic forces due to rotational motion, although we retain the aerodynamic moments that they generate, in the control design and analysis; the small aerodynamic forces are included in simulations.

For a given (constant) air density ρ and wing planform area S, the aerodynamic force expressed in the body reference frame can be written as:

$$\boldsymbol{f}_a(\boldsymbol{v}) = -\frac{1}{2}\rho S V^2 \mathbf{R}_{\mathrm{BW}}(\alpha,\beta)\boldsymbol{C}(\alpha,\beta) \tag{9}$$

where $\boldsymbol{C}(\alpha,\beta) = [C_D(\alpha,\beta), C_S(\alpha,\beta), C_L(\alpha,\beta)]^T$ contains the indicated nondimensional aerodynamic force coefficients. These are assumed to exhibit the following properties:

1) The drag coefficient, $C_D(\alpha,\beta)$, is a positive function and even in both arguments.
2) The side force coefficient, $C_S(\alpha,\beta)$, is a smooth, odd function with respect to β. It is positive (respectively, negative) when $e^{i\beta}$ lies in the first (respectively, fourth) quadrant of the complex plane.[1]
3) The lift coefficient, $C_L(\alpha,\beta)$, is a smooth function and nondecreasing with respect to α.

Although the third condition given above allows a diminishing slope of the lift coefficient near the stall angle of attack, it prohibits the decrease in lift coefficient that occurs with increasing angle of attack beyond the stall condition. Thus, while the aerodynamic model is quite general in its representation of normal flight conditions, the subsequent analysis and results require (and help to ensure) that the aircraft operates below the stall condition.

[1]Note that the sign of C_S is opposite the standard convention for lateral force coefficient.

Using the definitions of aerodynamic angles in equations (4) and (5), we can reformulate the aerodynamic forces:

$$\boldsymbol{f}_a(\boldsymbol{v}) = -\varrho \begin{bmatrix} u\mathrm{V}C_D - \dfrac{uvV}{\sqrt{u^2+w^2}}C_S - \dfrac{wV^2}{\sqrt{u^2+w^2}}C_L \\ v\mathrm{V}C_D + V\sqrt{u^2+w^2}C_S \\ w\mathrm{V}C_D - \dfrac{vwV}{\sqrt{u^2+w^2}}C_S + \dfrac{uV^2}{\sqrt{u^2+w^2}}C_L \end{bmatrix} \tag{10}$$

where $\varrho = 1/2\rho S$ is assumed to be constant and the drag, side-force and lift coefficients depend on the velocity $\boldsymbol{v}$. Equation (10) can be further decomposed as follows:

$$\boldsymbol{f}_a(\boldsymbol{v}) = \left(\hat{\boldsymbol{J}}_v - \mathcal{R}_v\right)\boldsymbol{v} \tag{11}$$

where $\boldsymbol{J}_v = (\varrho V)/((u^2+w^2)^{1/2})[wC_S, \mathrm{V}C_L, -uC_S]^T$ accounts for a force orthogonal to the velocity vector (i.e., a turning force) and where the matrix $\mathcal{R}_v = \varrho \mathrm{V} C_D \mathbb{I} \succ 0$ accounts for the dissipation of translational kinetic energy. (The term $\mathbb{I}$ represents the 3×3 identity matrix).

Let $\boldsymbol{\eta} = [\boldsymbol{\zeta}^T, \psi, \boldsymbol{q}^T]^T$ be the configuration vector, where $\boldsymbol{q}$ denotes the position of the aircraft in inertial space. We concatenate configuration and momentum into the state vector $\boldsymbol{x} = [\boldsymbol{h}^T, \boldsymbol{p}^T, \boldsymbol{\eta}^T]^T$.

Proposition 1: The system dynamics (6), (7), and (8) can be written in the PHS form (1-2) with Hamiltonian

$$\mathcal{H} = \frac{1}{2}\boldsymbol{h}^T \boldsymbol{I}^{-1}\boldsymbol{h} + \frac{1}{2m}\boldsymbol{p}^T\boldsymbol{p} - mg\boldsymbol{e}_3^T\boldsymbol{q} \tag{12}$$

and with

$$\mathcal{J} = \begin{bmatrix} \hat{\boldsymbol{h}} & \hat{\boldsymbol{p}} & \hat{\boldsymbol{\zeta}} & -\boldsymbol{a}(\boldsymbol{\zeta})^T & \mathbf{0} \\ \hat{\boldsymbol{p}} & \hat{\boldsymbol{J}}_v & \mathbf{0} & \mathbf{0} & -\mathbf{R}_{\mathrm{IB}}^T \\ \hat{\boldsymbol{\zeta}} & \mathbf{0} & \mathbf{0} & \mathbf{0} & \mathbf{0} \\ \boldsymbol{a}(\boldsymbol{\zeta}) & \mathbf{0} & \mathbf{0} & 0 & \mathbf{0} \\ \mathbf{0} & \mathbf{R}_{IB} & \mathbf{0} & \mathbf{0} & \mathbf{0} \end{bmatrix} \tag{13}$$

$$\mathcal{R} = \begin{bmatrix} \boldsymbol{D}_\omega & \mathbf{0} & \mathbf{0} & \mathbf{0} & \mathbf{0} \\ \mathbf{0} & \mathcal{R}_v & \mathbf{0} & \mathbf{0} & \mathbf{0} \\ \mathbf{0} & \mathbf{0} & \mathbf{0} & \mathbf{0} & \mathbf{0} \\ \mathbf{0} & \mathbf{0} & \mathbf{0} & 0 & \mathbf{0} \\ \mathbf{0} & \mathbf{0} & \mathbf{0} & \mathbf{0} & \mathbf{0} \end{bmatrix}, \quad \boldsymbol{g} = \begin{bmatrix} \mathbb{I} & \mathbf{0} \\ \mathbf{0} & \dfrac{\boldsymbol{v}}{V} \\ \mathbf{0} & \mathbf{0} \\ 0 & \mathbf{0} \\ \mathbf{0} & \mathbf{0} \end{bmatrix}^T. \tag{14}$$

Here, $\mathbf{R}_{\mathrm{IB}}$ depends on both $\boldsymbol{\zeta}$ and ψ and $\boldsymbol{a}(\boldsymbol{\zeta})$ is derived from equation (6): $\boldsymbol{a}(\boldsymbol{\zeta}) = -(1-\zeta_1^2)^{-1}\boldsymbol{\zeta}^T\hat{\boldsymbol{e}}_1\hat{\boldsymbol{e}}_1$. Note that this PHS formulation holds for aerodynamic coefficients C_D, C_S, and C_L of any functional form.

IV. Directional Stabilization

The procedure followed in this brief is inspired by the work of Fujimoto *et al.* [21], whose brief describes a trajectory tracking control strategy for PHSs in which a passive error dynamic system is constructed via canonical transformation.

The goal in this section is to stabilize the aircraft's motion to non-slipping ($\beta = 0$), wings-level ($\phi = 0$) flight in a specified direction described by a desired course angle χ_d and a desired climb angle γ_d, with $\gamma_d \neq \pm\pi/2$.

Rather than specify the desired airspeed V_d and solve for the desired angle of attack α_d, we specify the desired angle of attack and solve for the corresponding airspeed. The former approach would require knowing the functional forms for the aerodynamic force coefficients; we assume that only the most general properties of these functions are known. Directly specifying the desired angle of attack also allows one to more easily avoid the stall condition, which is not captured by the assumptions concerning the lift coefficient C_L. The stall is avoided through the judicious choice of the nominal flight condition and prescribed bounds on the initial state; see the discussion following Theorem 1.

The desired velocity vector is $\boldsymbol{v}_d = V_d(\cos\alpha_d, 0, \sin\alpha_d)^T$. Given a desired climb angle, selecting α_d also fixes the desired pitch angle, or equivalently the desired tilt vector since the desired roll angle is zero: $\boldsymbol{\zeta}_d = [-\sin(\alpha_d + \gamma_d),\ 0,\ \cos(\alpha_d + \gamma_d)]^T$. The angular velocity is zero in the desired state of steady, wings level flight at a fixed attitude. As for the translational velocity, the airspeed is chosen in such a way that the aerodynamic forces balance the component of gravitational force along the vertical axis. Therefore, $V_d = ((mg\cos\gamma_d)/(\varrho C_{L_d})^{1/2})$, where C_{L_d} is the lift coefficient evaluated at steady state, is chosen.

While $\boldsymbol{v}_d$ represents the desired velocity when the attitude is at a steady state, using it as the direct reference command may yield poor performance and violate conditions required in the proof of stability. Instead, state-dependent target values denoted with the subscript "t" are designed which converge to the desired values at a steady state.

Define the function

$$\mathcal{H}_c = \frac{1}{2}(\boldsymbol{h} - \boldsymbol{I}\boldsymbol{\omega}_t)^T \boldsymbol{I}^{-1}(\boldsymbol{h} - \boldsymbol{I}\boldsymbol{\omega}_t) + \frac{m}{2}(V - V_t)^2 + \mathcal{V}_d + \frac{mV_d^2}{2}\big((\sin\alpha - \sin\alpha_d)^2 + 2(1 - \cos\beta)\big) \tag{15}$$

where $\mathcal{V}_d = 1/2(k_\zeta(\boldsymbol{\zeta} - \boldsymbol{\zeta}_d)^T(\boldsymbol{\zeta} - \boldsymbol{\zeta}_d) + k_\psi(\psi - \psi_d)^2)$ is an artificial potential with $k_\zeta, k_\psi > 0$ and where

$$\boldsymbol{\omega}_t(\alpha, \beta, \boldsymbol{\zeta}) = \big[-gV_t^{-1}\zeta_2 \csc\alpha_d \cos\beta,\ 0,\ 0\big]^T \tag{16}$$

and

$$V_t(\alpha, \beta, \boldsymbol{\zeta}) = \sqrt{\frac{mg}{\varrho C_{L_d}}\left(\boldsymbol{e}_3^T \mathbf{R}_{\mathrm{BW}}^T \boldsymbol{\zeta} + \frac{\zeta_2 \sin 2\beta}{2\sin\alpha_d}\left(\cos\alpha - \frac{\cos\beta}{\cos\alpha}\right)\right)}. \tag{17}$$

Note that $\mathcal{H}_c$ can be split into $\mathcal{H}_h = 1/2(\boldsymbol{h} - \boldsymbol{I}\boldsymbol{\omega}_t)^T \boldsymbol{I}^{-1}(\boldsymbol{h} - \boldsymbol{I}\boldsymbol{\omega}_t)$ which contains information about error in the rotational dynamics, $\mathcal{V}_d$ which quantifies the error in the pitch and heading, and $\mathcal{H}_p = \mathcal{H}_c - \mathcal{H}_p - \mathcal{V}_d$ which contains information about error in the translational dynamics. Here and below, the velocity components V, α, and β should be interpreted as functions of the translational momentum $\boldsymbol{p}$.

Theorem 1: The control law

$$\boldsymbol{\tau}_{\mathrm{c}} = -\left[\mathbb{I} - \boldsymbol{I}\tfrac{\partial\boldsymbol{\omega}_{\mathrm{t}}}{\partial\boldsymbol{p}} \ -\boldsymbol{I}\tfrac{\partial\boldsymbol{\omega}_{\mathrm{t}}}{\partial\boldsymbol{\eta}}\right](\mathcal{J} - \mathcal{R})\frac{\partial\tilde{\mathcal{H}}}{\partial\boldsymbol{x}}^{\mathrm{T}} - \mathcal{C}(\boldsymbol{\omega} - \boldsymbol{\omega}_{\mathrm{t}}) - \boldsymbol{I}\frac{\partial\boldsymbol{\omega}_{\mathrm{t}}}{\partial\boldsymbol{x}}(\mathcal{J} - \mathcal{R})^{\mathrm{T}}\left[\mathbf{0}\ \tfrac{\partial\mathcal{H}_p}{\partial\mathbf{p}}\ \tfrac{\partial(\mathcal{V}_{\mathrm{d}} + \mathcal{H})}{\partial\boldsymbol{x}}\right]^{\mathrm{T}}, \tag{18}$$

$$F_{\mathrm{c}} = \varrho C_D V_{\mathrm{t}}^2 + m\left[\mathbf{0}, \frac{\partial V_{\mathrm{t}}}{\partial\boldsymbol{p}}, \frac{\partial V_{\mathrm{t}}}{\partial\boldsymbol{\eta}}\right](\mathcal{J} - \mathcal{R})\left[\boldsymbol{\omega}_{\mathrm{t}}^{\mathrm{T}}, \boldsymbol{v}^{\mathrm{T}}, \frac{\partial\mathcal{V}}{\partial\boldsymbol{\eta}}\right]^{\mathrm{T}} - mg\boldsymbol{v}^{\mathrm{T}}\boldsymbol{\zeta}V^{-1} + V_{\mathrm{d}}^2\big(mg(VV_{\mathrm{t}})^{-1}\sin\beta\zeta_2\cos\beta + \sec\beta\cos\alpha(\sin\alpha - \sin\alpha_{\mathrm{d}}) \cdot\big(mg(VV_{\mathrm{t}})^{-1}\boldsymbol{e}_3^{\mathrm{T}}\boldsymbol{R}_{\mathrm{BW}}^{\mathrm{T}}\boldsymbol{\zeta} - \varrho C_{L_{\mathrm{d}}}\big)\big), \tag{19}$$

where $\tilde{\mathcal{H}} = \mathcal{H} - \mathcal{H}_c$ and $\mathcal{C} \succ 0$, asymptotically stabilizes the desired equilibrium.

Remark 1: Implementing the control law requires knowledge of the aerodynamic model, but the proof does not rely on an explicit functional form for the aerodynamic forces and moments. See the comments following (9).

Proof: Taking $\mathcal{H}_c$ as a candidate Lyapunov function,

$$\dot{\mathcal{H}}_c = \frac{\partial\mathcal{H}_c}{\partial\boldsymbol{x}}\left((\mathcal{J} - \mathcal{R})\frac{\partial\mathcal{H}}{\partial\boldsymbol{x}}^T + \boldsymbol{g}\boldsymbol{u}\right) = \frac{\partial\mathcal{H}_c}{\partial\boldsymbol{x}}\left((\mathcal{J} - \mathcal{R})\frac{\partial\tilde{\mathcal{H}}}{\partial\boldsymbol{x}}^T + \boldsymbol{g}\boldsymbol{u}\right) - \frac{\partial\mathcal{H}_c}{\partial\boldsymbol{x}}\mathcal{R}\frac{\partial\mathcal{H}_c}{\partial\boldsymbol{x}}^T. \tag{20}$$

With the proposed control moment, $\boldsymbol{\tau}_c$, in equation (18), the time derivative of the proposed Hamiltonian function becomes:

$$\dot{\mathcal{H}}_c = -\frac{\partial\mathcal{H}_c}{\partial\boldsymbol{x}}\mathcal{R}\frac{\partial\mathcal{H}_c}{\partial\boldsymbol{x}}^T - (\boldsymbol{\omega} - \boldsymbol{\omega}_t)^T\mathcal{C}(\boldsymbol{\omega} - \boldsymbol{\omega}_t) + \begin{bmatrix}\mathbf{0}\\ \frac{\partial\mathcal{H}_p}{\partial\boldsymbol{p}}^T\\ \frac{\partial\mathcal{V}_d}{\partial\boldsymbol{\eta}}^T + \frac{\partial\mathcal{H}_p}{\partial\boldsymbol{\eta}}^T\end{bmatrix}^T(\mathcal{J} - \mathcal{R})\begin{bmatrix}\boldsymbol{\omega}_t\\ \boldsymbol{v} - \frac{\partial\mathcal{H}_p}{\partial\boldsymbol{p}}^T\\ \frac{\partial\mathcal{V}}{\partial\boldsymbol{\eta}}^T - \frac{\partial\mathcal{V}_d}{\partial\boldsymbol{\eta}}^T - \frac{\partial\mathcal{H}_p}{\partial\boldsymbol{\eta}}^T\end{bmatrix}. \tag{21}$$

Adding and subtracting the term $(\partial\mathcal{H}_p)/(\partial\boldsymbol{x})(\mathcal{J} - \mathcal{R})(\partial\mathcal{H}_p)/(\partial\boldsymbol{x})^T$ and taking advantage of the structure of $\mathcal{J}$ and $\mathcal{R}$ reduces equation (21) to

$$\dot{\mathcal{H}}_c = -\frac{\partial\mathcal{H}_h}{\partial\boldsymbol{x}}\mathcal{R}\frac{\partial\mathcal{H}_h}{\partial\boldsymbol{x}}^T - (\boldsymbol{\omega} - \boldsymbol{\omega}_t)^T\mathcal{C}(\boldsymbol{\omega} - \boldsymbol{\omega}_t) + \begin{bmatrix}\mathbf{0}\\ \frac{\partial\mathcal{H}_p}{\partial\boldsymbol{p}}^T\\ \frac{\partial\mathcal{V}_d}{\partial\boldsymbol{\eta}}^T + \frac{\partial\mathcal{H}_p}{\partial\boldsymbol{\eta}}^T\end{bmatrix}^T(\mathcal{J} - \mathcal{R})\begin{bmatrix}\boldsymbol{\omega}_t\\ \boldsymbol{v}\\ \frac{\partial\mathcal{V}}{\partial\boldsymbol{\eta}}^T\end{bmatrix}. \tag{22}$$

Expanding (22) and substituting for the control thrust F_c from equation (19) gives:

$$\begin{aligned}\dot{\mathcal{H}}_c = {} & -\frac{\partial\mathcal{H}_h}{\partial\boldsymbol{x}}\mathcal{R}\frac{\partial\mathcal{H}_h}{\partial\boldsymbol{x}}^T - (\boldsymbol{\omega} - \boldsymbol{\omega}_t)^T\mathcal{C}(\boldsymbol{\omega} - \boldsymbol{\omega}_t)\\ & - \varrho C_D(V - V_t)\big(V^2 - V_t^2\big)\\ & + k_\zeta(\boldsymbol{\zeta} - \boldsymbol{\zeta}_d)^T\hat{\boldsymbol{\zeta}}\boldsymbol{\omega}_t + k_\psi(\psi - \psi_d)\boldsymbol{a}(\boldsymbol{\zeta})\boldsymbol{\omega}_t\\ & + V_d^2\sin\beta\big(mgV_t^{-1}\zeta_2\cos\beta - \varrho VC_S - m\boldsymbol{e}_3^T\boldsymbol{R}_{\mathrm{BW}}\boldsymbol{\omega}_t\\ & \qquad - mgV^{-1}\sin\beta(\zeta_1\cos\alpha + \zeta_3\sin\alpha)\big)\\ & + V_d^2(\sin\alpha - \sin\alpha_d)\cos\alpha\sec\beta\\ & \big(-\varrho V_t C_L + m\boldsymbol{e}_2^T\boldsymbol{R}_{\mathrm{BW}}\boldsymbol{\omega}_t + mgV_t^{-1}\boldsymbol{e}_3^T\boldsymbol{R}_{\mathrm{BW}}\boldsymbol{\zeta}\big).\end{aligned} \tag{23}$$

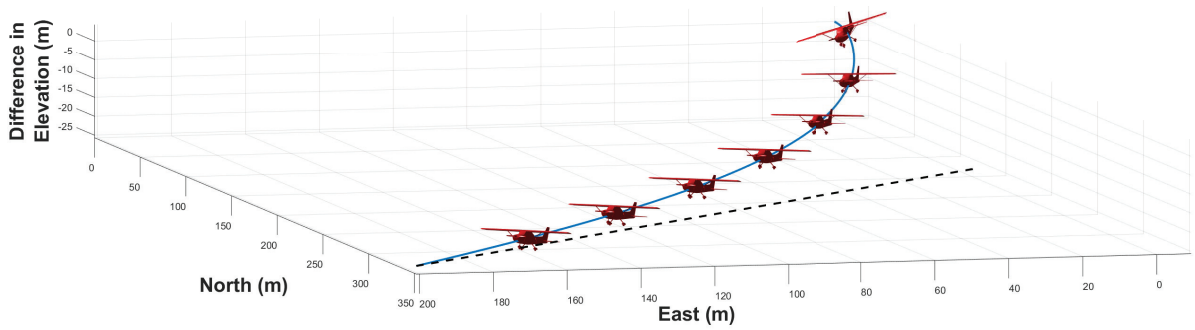

Fig. 2. Desired velocity direction (black dashed) and actual path (blue solid). The initial position is the origin. Vehicle attitude is denoted at two second intervals by the 3-D aircraft model.

One may use ω_{1_t} to eliminate undesired terms involving $V_d \sin\beta$. However, ω_{1_t} is multiplied by $\sin\alpha$ whose value can pass through zero during transient motion. To resolve this issue, subtract $V_d^2 \sin\beta(\sin\alpha - \sin\alpha_d) m\boldsymbol{\omega}_{1_t}$ from the fourth line of (23) and add it to the last line. Substituting (16) and (17) in (23) then gives:

$$\begin{aligned}\dot{\mathcal{H}}_c = &-\frac{\partial \mathcal{H}_h}{\partial \boldsymbol{x}} \mathcal{R} \frac{\partial \mathcal{H}_h}{\partial \boldsymbol{x}}^T - (\boldsymbol{\omega} - \boldsymbol{\omega}_t)^T \mathcal{C}(\boldsymbol{\omega} - \boldsymbol{\omega}_t) \\ &- \varrho C_D (V - V_t)^2 (V + V_t) - \frac{g\zeta_2^2 \zeta_{3_d} \cos\beta}{V_t \sin\alpha_d} \\ &- \frac{V_d^2 \sin\beta}{V} \big(\varrho V^2 C_S + mg \sin\beta(\zeta_1 \cos\alpha + \zeta_3 \sin\alpha)\big) \\ &- \frac{\varrho V_t V_d^2 (\sin\alpha - \sin\alpha_d)\big(C_L - C_{L_d}\big)\cos\alpha}{\cos\beta}. \end{aligned} \tag{24}$$

Note that the first two terms are non-positive since $\mathcal{R} \succeq 0$ and $\mathcal{C} \succ 0$. In addition, the facts that C_D is positive and that V and V_t are non-negative mean that $-\varrho C_D (V - V_t)^2 (V + V_t) \leq 0$. The term $-(V_d^2 \sin^2\beta)/V(\zeta_1 \cos\alpha + \zeta_3 \sin\alpha)$ is not guaranteed to be nonpositive, however $|\sin^2\beta(\zeta_1 \cos\alpha + \zeta_3 \sin\alpha)| \leq 1$. Provided the airspeed $V > 0$ remains sufficiently large, this term will not affect the sign definiteness of $\dot{\mathcal{H}}_c$. The conditions for Lyapunov stability must hold within level sets of $\mathcal{H}_c$. By choosing a sufficiently small level set, one can ensure that V remains sufficiently large and therefore that $\dot{\mathcal{H}}_c \leq 0$, showing that the desired equilibrium is stable.

LaSalle's principle states that trajectories which begin in a compact and positively invariant set $\boldsymbol{\Omega}$, where the Lyapunov conditions hold, converge to the largest invariant set M contained in the set $E = \{(\boldsymbol{h}, \boldsymbol{p}, \boldsymbol{\zeta}, \psi) \subset \boldsymbol{\Omega} \mid d/(dt)\mathcal{H}_c = 0\}$. It can be easily shown that $d/(dt)\mathcal{H}_c = 0$ if and only if $\boldsymbol{\omega} = \boldsymbol{0}$, $V = V_t$, $\alpha = \alpha_d$, $\beta = 0$ and $\zeta_2 = 0$. Depending on the set $\boldsymbol{\Omega}$, however, there could be more than one state contained within M. To determine all possible states contained in M, one must consider the dynamics within the set E. Referring to equations (6), (7), and (8), we find that the equations are satisfied if and only if $\boldsymbol{\zeta} = \boldsymbol{\zeta}_d$ and $\psi = \psi_d$. The equilibrium is therefore (locally) asymptotically stable. To estimate the basin of attraction, one may examine level sets of the Lyapunov function.

Remark 2: In applications where energy shaping is used to stabilize a PHS, one typically shows that the closed-loop dynamics are Hamiltonian with respect to a control-modified Hamiltonian, and then proceeds with stability analysis. For the fixed-wing nonlinear flight control problem considered here, we were unable to obtain a coordinate transformation under which the closed-loop dynamics can be recognized as a Hamiltonian system. Doing so requires solving a system of partial differential equations (PDEs) whose solution is not intuitive, even when the functional form of the aerodynamic force coefficients is explicit. In our case, we consider a general class of aerodynamic force coefficients and show, in the proof of Theorem 1, that the function $\mathcal{H}_c$ is indeed a Lyapunov function.

V. Simulation

To demonstrate the control law presented earlier, we simulate its performance using a flight dynamic model for the T-2 generic transport model (GTM) presented in [24].

In the simulation, the aircraft starts with an airspeed of 20 m/s and with initial values of zero for α and β. The desired motion corresponds to wings-level flight at an angle of attack of 10° with a zero climb angle and a course angle of 45° (northeast). Initial values for state variables other than velocity were chosen randomly. The results shown in Fig. 2 reflect the analytical stability results presented earlier, although the simulation model incorporates aerodynamic interactions that were ignored in the control design and analysis, such as aerodynamic force terms involving angular rates.

Fig. 2 shows the vehicle trajectory (solid line) using the proposed controller subject to the previously stated initial conditions. The aircraft's orientation is indicated at equal time steps by a 3-D model of a conventional aircraft, although the geometry is not that of the GTM. The feedback-controlled trajectory converges to the desired flight profile. Figs. 3 and 4 show the time history of rates and attitude variables as solid lines and the corresponding desired steady-state values as dotted lines.

Additional simulations have been performed to explore the assumption that thrust is aligned with velocity. This assumption differs from the more common assumption that thrust is aligned with the longitudinal axis. While physical mechanisms are available to adjust the line of thrust, neither of these two assumptions is especially accurate for a generic aircraft with a fixed propulsor. In any case, to examine the sensitivity of the stability results to the thrust direction

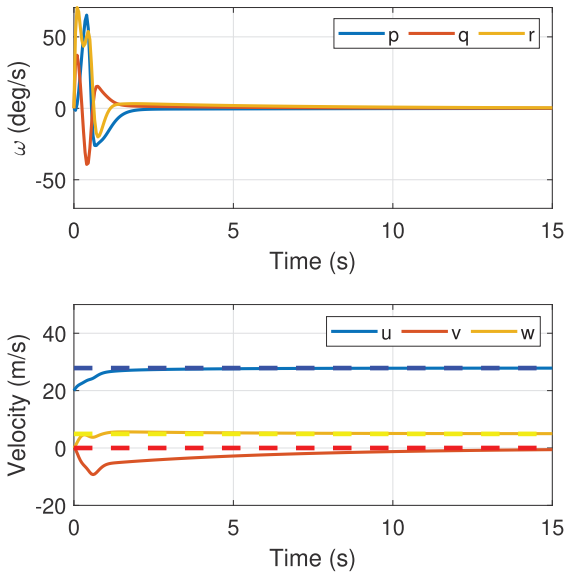

Fig. 3. Desired (dashed) and actual (solid) both angular and translational velocity histories corresponding to Fig. 2.

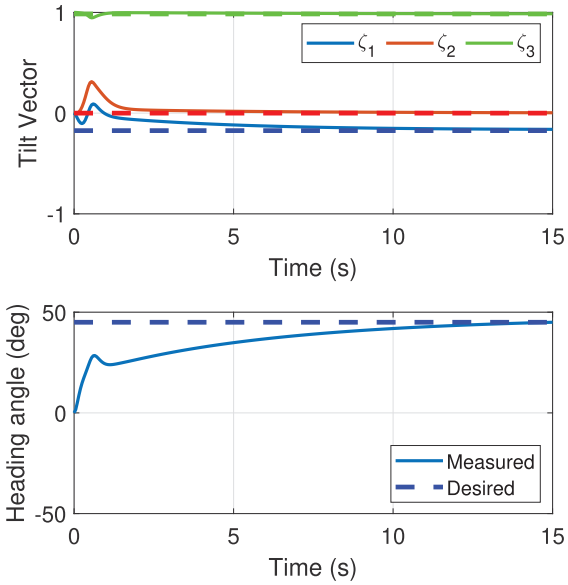

Fig. 4. Desired (dashed) and actual (solid) attitude histories corresponding to Fig. 2.

and magnitude, we include two additional simulations—one for which the magnitude of the feedback-controlled thrust is directed along the longitudinal axis (constant thrust line with varying thrust) and another where the constant-magnitude thrust is applied along this same fixed thrust line. The time history of the Lyapunov function is shown in Fig. 5. The non-negative Lyapunov function decreases monotonically for the proposed control law, as it must do, and it appears to do the same when the (feedback-varying) commanded thrust magnitude is directed along the longitudinal axis. In the case of constant, longitudinal thrust, the aircraft motion converges to the desired one, however, the value of $\mathcal{H}_c$ does not decrease monotonically.

Further simulations were conducted to study the controller's behavior in the presence of uncertainties in the inertial

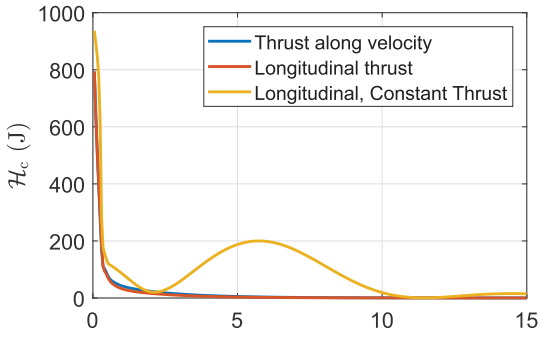

Fig. 5. Lyapunov function histories for different thrust scenarios.

parameters and the aerodynamic model. All the simulations begin with the initial state previously described and are prescribed the same desired steady-state as above with a simulation time of 40 s. The simulations indicate that the closed-loop performance is robust to the uncertainties in the sense that the system remains stable and the state converges to a steady motion in the neighborhood of the desired motion. To quantify the effect of perturbations, an appropriate metric was defined. First, we define the mean squared deviation P of the velocity direction from the desired value for the perturbed flight dynamic model:

$$P = \frac{1}{T_s}\int_0^{T_s}\left(\frac{\mathbf{R}_{\mathbb{IB}}(t)\boldsymbol{p}(t)}{\|\boldsymbol{p}(t)\|} - \boldsymbol{i}_d\right)^T\left(\frac{\mathbf{R}_{\mathbb{IB}}(t)\boldsymbol{p}(t)}{\|\boldsymbol{p}(t)\|} - \boldsymbol{i}_d\right)dt \quad (25)$$

where $\boldsymbol{i}_d = e^{-\chi_d \hat{\boldsymbol{e}}_3} e^{-\gamma_d \hat{\boldsymbol{e}}_2}\boldsymbol{e}_1$ is the desired inertial velocity direction and T_s is the total simulation time. We define N similarly as the mean squared deviation of the velocity direction for the nominal plant. The error metric is

$$E = \left|\frac{P - N}{N}\right|. \quad (26)$$

To better understand the effectiveness of the controller compared to other approaches, we consider an alternative control design approach. Since the control law developed here involves static state feedback, we compare it with another nonlinear static state feedback method. The dynamic inversion controller described in [25] is chosen due to its popularity and ease of implementation. In line with the methodology detailed in the brief, a "control output" vector of the same dimensions as the input vector is taken. To present a fair comparison between the passivity-based and dynamic inversion controllers, the control input vector is selected to reflect quantities present in the control Hamiltonian in equation (15): $\bar{\boldsymbol{y}} = [\alpha - \alpha_d, \beta, \zeta_1 + \sin\alpha_d, \psi - \psi_d]^T$. Each element in the control output vector is differentiated, with respect to time, until at least one element of the control input vector appears. Hence, for each element of the output vector, $\bar{y}_i$, one obtains an equation of the form $\bar{y}_i^{(d_i)} = b_i + \boldsymbol{B}_i\boldsymbol{u}$, where the superscript (d_i) denotes the number d_i of time derivatives that are taken, b_i is the sum of all the terms that are independent of the input, and $\boldsymbol{B}_i$ is a row vector representing whether and how the various input components appear in the given derivative of $\bar{\boldsymbol{y}}_i$. Let $\boldsymbol{b}$ be the vector formed by concatenating all the b_i's and $\boldsymbol{B}$ be the matrix constructed by stacking all the $\boldsymbol{B}_i$'s. The inverse dynamics control law is $\boldsymbol{u} = -\boldsymbol{B}^{-1}(\boldsymbol{b} + \boldsymbol{v})$, where

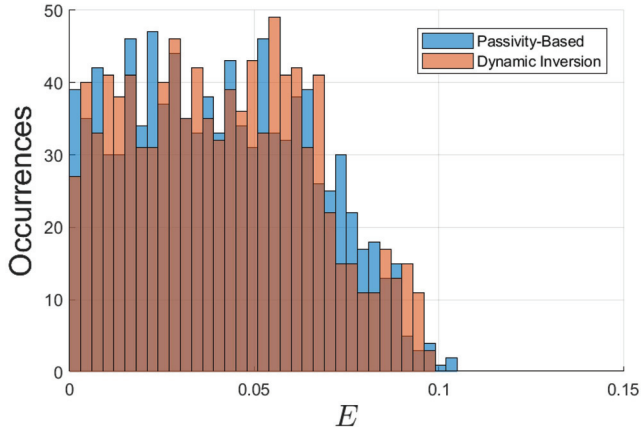

Fig. 6. Histogram comparing performance of the passivity-based and dynamic inversion controllers for 1000 simulations with uncertain inertia parameters.

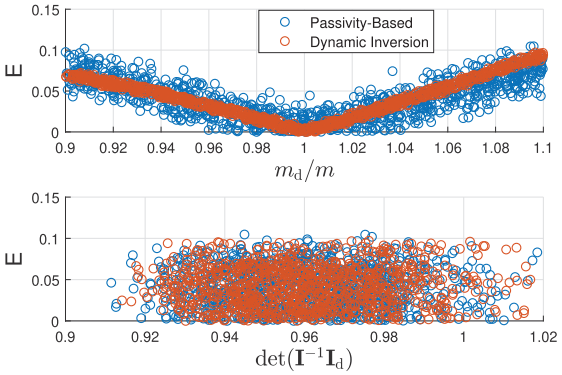

Fig. 7. Performance comparison of the passivity-based and dynamic inversion controllers, given uncertainty in the aircraft's mass (top) and inertia (bottom). The subscript "d" indicates the terms with perturbation.

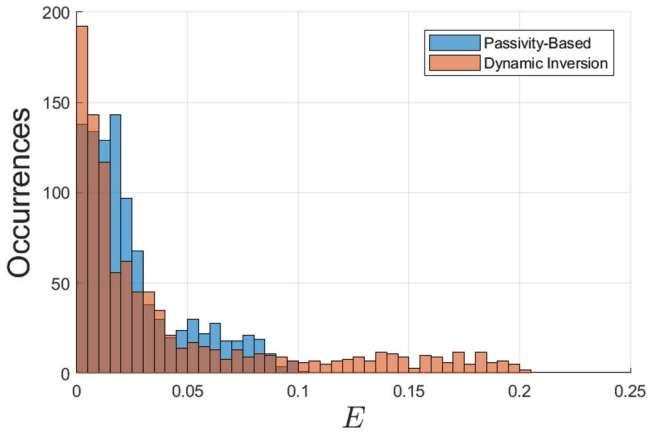

Fig. 8. Histogram comparing performance of the passivity-based and dynamic inversion controllers for 1000 simulations with uncertain aerodynamic parameters.

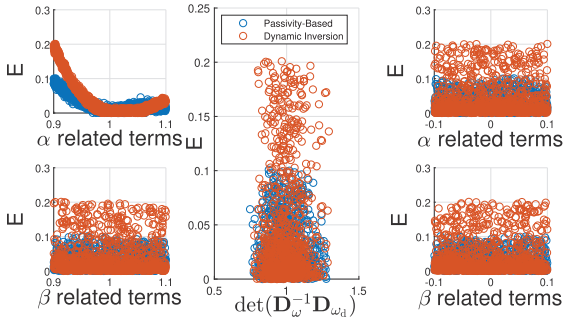

Fig. 9. Performance comparison of the passivity-based and dynamic inversion controllers, given uncertainty in the aerodynamic force (left), aerodynamic moment due to rotational velocity (middle), and aerodynamic moment due to translational velocity (right). The subscript "d" indicates the terms with perturbation.

$\boldsymbol{v} = \sum_{k=0}^{d-1} \boldsymbol{P}_k \bar{\boldsymbol{y}}^{(k)}$. Here, $\boldsymbol{P}_k$ is a set of preselected, constant matrices. For the sake of this comparison study, the set $\boldsymbol{P}_k$ is selected to achieve a performance similar to that of the PBC.

A. Uncertainty in Inertial Parameters

For uncertainties in the inertial parameters, we consider perturbations to the mass and inertia matrix. For each simulation, these perturbations are randomly generated, with a uniform distribution ranging between $\pm 10\%$ of the corresponding term's nominal value. All other parameters are kept the same as before. The controllers are fed accurate translational and rotational velocities, as well as the position and attitude data, and compute the respective momenta, in addition to the required system inputs, using the nominal mass and inertia matrix. 1000 numerical simulations of the closed-loop system were conducted under these conditions for either controller. Results indicate that both controllers had a comparable performance where the state remains within a neighborhood of the desired steady state, as shown by the histogram in Fig. 6.

B. Uncertainty in Aerodynamic Model

The uncertainty in the aerodynamic model takes the form of perturbations to the aerodynamic coefficients. As before, the perturbations are generated at random in a uniform distribution ranging between $\pm 10\%$ of the corresponding term's nominal value. The aerodynamic model uncertainties that are considered fall in three categories: uncertainty in the aerodynamic force due to the translational velocity, uncertainty in the aerodynamic moment due to the angular velocity, and uncertainty in the aerodynamic moment due to the translational velocity. The first two sources act on terms and quantities already accounted for in the simulation model. With regard to aerodynamic moments due to translational velocity, recall that these terms were omitted from consideration with the understanding that their effect should later be removed from the computed control moment. The concept is akin to feedback linearization, so it is especially important to assess the effect of uncertainty in these terms. For expedience, the coefficients are classified as being related to the angle of attack (α-dominant) or being related to the sideslip angle (β-dominant). Then, the coefficients of the same class are perturbed by the same randomly generated number. Like before, 1000 numerical simulations of the closed-loop of system were conducted under these conditions for either controller. As shown by the histogram in Fig. 8, results show that the state remains within a neighborhood of the desired steady state. However, the tail of the distribution pertaining to dynamic inversion is much longer

than that for PBC. This observation suggests that the proposed controller is more robust to uncertainties in the aerodynamic model.

The simulation results also indicate that the performance of both controllers is more sensitive to perturbations in α-dominant terms than any other terms as shown in Fig. 9.

VI. Conclusion

This brief presents a nonlinear, energy-based control design for a small, fixed wing aircraft that stabilizes the aircraft to wings-level flight at a commanded velocity, characterized by a desired speed, course, and climb angle. The control law requires knowledge of some aerodynamic parameters, but the stability analysis uses very general assumptions about the aerodynamic forces and moments.

By recognizing a special structure of the aerodynamic force, it is possible to cast the aircraft equations of motion as a PHS. One may then leverage the system's passivity properties to design a nonlinear, energy-based control strategy. A Lyapunov function candidate was constructed by modifying the storage function; the stability proof relies on exploiting the structure of the PHS model. Simulations illustrate that the control law is robust to model parameter uncertainty and that its performance compares favorably with dynamic inversion, an alternative, nonlinear, static state feedback method.

Future work involves adapting the control law presented here to stabilize a time-varying desired velocity, which is a precursor for curvilinear path-following, and demonstrating the algorithm in flight tests.

Acknowledgment

The authors would like to thank the anonymous reviewers for their constructive feedback and Dr. Francis Valentinis for many fruitful conversations during his one-year study leave at Virginia Tech.

References

[1] S. A. Snell, D. F. Enns, and W. L. Garrard, "Nonlinear inversion flight control for a supermaneuverable aircraft," *J. Guid., Control, Dyn.*, vol. 15, no. 4, pp. 976–984, Jul. 1992.

[2] H. K. Khalil, *Nonlinear Systems*, 2nd ed. Upper Saddle River, NJ, USA: Prentice-Hall, 1996.

[3] S. Sastry, *Nonlinear Systems: Analysis, Stability, and Control*. New York, NY, USA: Springer, 2013.

[4] N. Hovakimyan and C. Cao, L_1 *Adaptive Control Theory: Guaranteed Robustness With Fast Adaptation*. Philadelphia, PA, USA: Society for Industrial and Applied Mathematics, 2010.

[5] M. Krstic, I. Kanellakopoulos, and P. V. Kokotovic," *Nonlinear and Adaptive Control Design*. Hoboken, NJ, USA: Wiley, 1995.

[6] K. J. Åström and B. Wittenmark, *Adaptive Control*. North Chelmsford, MA, USA: Courier Corporation, 2013.

[7] A. van der Schaft, *L2-Gain and Passivity Techniques in Nonlinear Control*, vol. 2. New York, NY, USA: Springer, 2000.

[8] R. Ortega and E. García-Canseco, "Interconnection and damping assignment passivity-based control: A survey," *Eur. J. Control*, vol. 10, no. 5, pp. 432–450, Jan. 2004.

[9] R. Ortega, A. van der Schaft, B. Maschke, and G. Escobar, "Interconnection and damping assignment passivity-based control of port-controlled Hamiltonian systems," *Automatica*, vol. 38, no. 4, pp. 585–596, Apr. 2002.

[10] H. González, M. A. Duarte-Mermoud, I. Pelissier, J. C. Travieso-Torres, and R. Ortega, "A novel induction motor control scheme using IDA-PBC," *J. Control Theory Appl.*, vol. 6, no. 1, pp. 59–68, Feb. 2008.

[11] J. A. Acosta, M. I. Sanchez, and A. Ollero, "Robust control of underactuated aerial manipulators via IDA-PBC," in *Proc. 53rd IEEE Conf. Decis. Control*, Dec. 2014, pp. 673–678.

[12] M. E. Guerrero, D. A. Mercado, R. Lozano, and C. D. Garcia, "IDA-PBC methodology for a quadrotor UAV transporting a cable-suspended payload," in *Proc. Int. Conf. Unmanned Aircr. Syst. (ICUAS)*, Jun. 2015, pp. 470–476.

[13] B. Yuksel, C. Secchi, H. H. Bulthoff, and A. Franchi, "Reshaping the physical properties of a quadrotor through IDA-PBC and its application to aerial physical interaction," in *Proc. IEEE Int. Conf. Robot. Autom. (ICRA)*, May 2014, pp. 6258–6265.

[14] A. Y. Mersha, R. Carloni, and S. Stramigioli, "Port-based modeling and control of underactuated aerial vehicles," in *Proc. IEEE Int. Conf. Robot. Autom.*, May 2011, pp. 14–19.

[15] L. E. Munoz, O. Santos, P. Castillo, and I. Fantoni, "Energy-based nonlinear control for a quadrotor rotorcraft," in *Proc. Amer. Control Conf.*, Jun. 2013, pp. 1177–1182.

[16] C. A. Woolsey and L. Techy, "Cross-track control of a slender, underactuated AUV using potential shaping," *Ocean Eng.*, vol. 36, no. 1, pp. 82–91, Jan. 2009.

[17] J.-M.-W. Fahmi and C. A. Woolsey, "Directional stabilization of a fixed-wing aircraft using potential shaping," in *Proc. Atmos. Flight Mech. Conf.*, Jun. 2018, p. 3620.

[18] F. Valentinis, A. Donaire, and T. Perez, "Energy-based motion control of a slender hull unmanned underwater vehicle," *Ocean Eng.*, vol. 104, pp. 604–616, Aug. 2015.

[19] F. Valentinis, A. Donaire, and T. Perez, "Energy-based guidance of an underactuated unmanned underwater vehicle on a helical trajectory," *Control Eng. Pract.*, vol. 44, pp. 138–156, Nov. 2015.

[20] F. Valentinis and C. Woolsey, "Nonlinear control of a subscale submarine in emergency ascent," *Ocean Eng.*, vol. 171, pp. 646–662, Jan. 2019.

[21] K. Fujimoto, K. Sakurama, and T. Sugie, "Trajectory tracking control of port-controlled Hamiltonian systems via generalized canonical transformations," *Automatica*, vol. 39, no. 12, pp. 2059–2069, Dec. 2003.

[22] B. Etkin, *Dynamics of Atmospheric Flight*. Mineola, NY, USA: Dover, 1972.

[23] T. Battista, S. Jung, C. Woolsey, and E. Paterson, "An energy-casimir approach to underwater vehicle depth and heading regulation in short crested waves," in *Proc. IEEE Conf. Control Technol. Appl. (CCTA)*, Aug. 2017, pp. 217–222.

[24] J. A. Grauer and E. A. Morelli, "A generic nonlinear aerodynamic model for aircraft," in *Proc. AIAA Atmos. Flight Mech. Conf.*, Jan. 2014, p. 542.

[25] S. H. Lane and R. F. Stengel, "Flight control design using non-linear inverse dynamics," *Automatica*, vol. 24, no. 4, pp. 471–483, Jul. 1988.